JOURNAL OF MATERIALS SCIENCE 21 (1986) 3601–3610

Craze microstructure characterization by low-angle electron diffraction and Fourier transforms of craze images

ARNOLD C.-M. YANG, EDWARD J. KRAMER
Department of Materials Science and Engineering and the Materials Science Center, Cornell University, Ithaca, New York 14853, USA

Craze microstructure in thin film monodisperse polystyrene (PS) was determined by three equivalent, but independent, techniques: (1) low-angle electron diffraction (LAED) from the crazes, (2) the image analysis of microdensitometer scans of craze TEM images, and (3) optical transforms of the TEM images. Molecular weights of 11×10^4 and 18×10^5 were investigated. The average craze fibril spacings and fibril diameters in the samples were measured by LAED and then compared with those obtained from the image analyses. Excellent agreement was found between the three techniques, indicating that any one can be used for craze fibril structure exploration. While the craze fibril structure near the craze–matrix interface of crazes in both the 18×10^5 and 11×10^4 were similar, the fibril structure was coarser in the centre of 11×10^4 crazes than in 18×10^5 crazes. This effect is believed to be due to fibril coalescence in the centre of the low molecular weight crazes during the very low strain rate tensile deformation used to produce those crazes.

1. Introduction

Fracture in glassy polymers usually is preceded by the appearance of crazes, localized zones of microdeformation, which can cause the low strain failure commonly observed in these materials [1–4]. Electron micrographs of crazes reveal them to be composed of many small fibrils aligned parallel to the applied maximum principal stress. The fibrils physically bridge between two interfaces with the undeformed bulk polymer and are load-bearing. The scale of the fibrils determines both the number of entangled polymer chains that must be disentangled or broken during, and the effective number of entangled chains in each fibril that survives, the fibrillation process. The former is thought to be an important factor in determining the crazing stress and craze growth kinetics [3, 5] and the latter is important in governing craze fibril breakdown [6].

The effects of the molecular weight, M, on polymer mechanical properties has long been noticed [7–13]. For example, the ultimate tensile strength increases rapidly with M in the range between 5 and 20×10^4 from very low values to much higher ones [13]. The craze fibril stability consistently shows a similar increase in exactly the same molecular weight range [6]. That transition signifies that the entanglement network in the amorphous polymer becomes effective in preventing the breakdown of craze fibrils in that range of molecular lengths. It is thus of interest to measure any changes in craze fibril structure that occur over this range of molecular weight [3, 14–16].

To explore the craze fibril structure the techniques of transmission electron microscopy (TEM), small-angle X-ray scattering (SAXS), and low-angle electron diffraction (LAED) have been used previously. Because it is able to obtain high-resolution craze images, TEM has been used extensively. Since, however, the craze fibril structure in a polymer film thick enough to produce crazes characteristic of bulk polymer consists of a forest of fibrils, it is difficult to resolve individual fibrils, or spacings between fibrils, on the projected image. Typical crazes also usually have a wide distribution of fibril diameters, D, and fibril spacings, D_0, so to obtain reliable moments of that distribution from stereo TEM images is extremely tedious [17]. To overcome this difficulty, small-angle X-ray scattering (SAXS) was invoked to study the crazes, but only in the bulk samples. Paredes and Fischer [18], as well as Brown and Kramer [19] have used the Porod analysis to determine the average fibril diameter of crazes. More recently, Brown [20] demonstrated that low-angle electron diffraction (LAED) can be used to obtain the same information for crazes in thin films and the analysis used for SAXS data could be employed for this novel technique. The LAED method, first developed by Mahl and Weitsch [21–23], and Ferrier [24] in the early 1960s by making use of the conventional electron microscope as a diffraction camera, can obtain diffraction patterns of very high angular resolution from a small area (as small as 10 μm diameter). The fact that TEM electron images from the same areas can be acquired virtually simultaneously, means that image information can be used to guide the interpretation of the LAED pattern. LAED is thus an attractive tool for determining the microstructure in thin films.

0022–2461/86 $03.00 + .12

However, the controversial inelastic "background" intensity at the very low angles [24–26] poses a problem in using LAED on thin film crazes. If the background is dependent on angle, the inelastic background should be excluded before a full quantitative approach like that used in SAXS can be undertaken. Yet, from the theory available to date, a description of the effects of the inelastic scattering on the LAED pattern is still quite vague.

It is generally agreed [27] that the electrons from the incident beam can dissipate a fraction of their kinetic energy by exciting the outer-shell electrons collectively (plasmon excitation) or individually (intra- or inter-"band" transitions). The theoretical calculation of Lenz [28] in 1954 predicts that the inelastic scattering cross-section of carbon, for example, is around five orders of magnitude larger than the elastic scattering cross-section at the angles below 10^{-4} radian. Nevertheless the energy loss of the incident electrons which are involved in this scattering is very small, (typically ~ 10 eV), compared to the total, say 200 keV. And even though the electron wave may have lost some energy it may still maintain coherence or the ability to interfere with itself. The diffuse scattering of the inelastic electrons, therefore, might be sharply peaked at the Bragg reflection positions just like the elastic scattering except that the effective atomic scattering factor falls off more rapidly with angle because of the larger scattering centres involved in the excitation [27].

Usually the inelastic electrons can be detected and excluded by setting a retarding field electron filter *in situ* when the LAED pattern is scanned by an electron detector [24]. In this fashion, a diffraction curve with a set limit of energy loss can be acquired. Tompsett *et al.* [29], among other workers, used this technique to show that an intense angular dependent inelastic background exists at low angles which degrades the LAED patterns of a silver film on a carbon substrate. Yet, Curtis and Ferrier [30] using the same technique revealed that only very small amount of inelastic scattering background was present in the electron scattering from the heavy-atom-coated carbon optical grating. The phase modulation induced by the periodic variation in specimen thickness was used by them in their attempt to explain this result. Thus it seems clear that a universal view of the inelastic background, supported both by the theory and experimental data, is not yet within our grasp.

For the purpose of craze microstructure determination, however, we approach this problem from a different direction. Previously [31] we used LAED to show that the average fibril spacing and diameter or thin film crazes are comparable with those of crazes in the bulk determined by SAXS, which is influenced to a negligible extent by inelastic scattering. In this paper we investigate this problem further by comparing the craze fibril structure obtained by LAED with that extracted from the image itself, which is free from the background problem. Fourier transforms of the optical density distribution on craze TEM negatives and optical transforms from the masks made of craze TEM plates were performed and the results are compared with those from LAED.

2. Experimental procedure

Thin film polymer specimens were prepared by following the method developed by Lauterwasser and Kramer [32]. Polystyrene (PS) was dissolved into toluene and uniform PS thin films of thickness 400 nm were cast on glass microscope slides by drawing these from a PS solution at a constant speed. The film was floated off the slide on to the surface of a water bath and picked up on a ductile copper mesh with a grid size about 1 mm × 1 mm. The grid bars of the copper mesh had been previously coated with a thin layer of PS by dipping the copper grid into the PS solution. A short exposure of the film to toluene vapour removed any slack in the film and caused the film to adhere to the grid bars. The residual solvent was then removed by placing the specimens in vacuum at room temperature for at least 35 h.

A starter crack, 120 μm long, was burned into the centre of each film square using the intense focused beam of an electron microprobe [33]. These cracks provided reproducible sites for craze nucleation. Crazes could be grown from the tips of the starter crack by mounting the copper grid in a strain frame and straining it at a constant low strain rate of $5 \times 10^{-7}\,\mathrm{sec}^{-1}$. Each individual square could be observed using an optical microscope and a suitable square could be cut from the deformed copper grid for immediate observation by TEM. Since the copper is deformed plastically, the crazes in the film square were thus examined in the unrelaxed state, under tensile stress.

Low-angle electron diffraction (LAED) was carried out by using a JEOL 200CX electron microscope operating at 200 kV. The longest camera length, 62.6 m, and the smallest beam size, spot 4, were used. An objective aperture, 20 μm diameter, which served as the selected-area aperture, was centred within a section of wide craze to produce the LAED patterns which were recorded on films. The microscope was then switched to the image mode to record the TEM image of the same craze. The camera length was calibrated using a carbon wafer grating of 416 nm spacing. The calibration LAED pattern shows that the primary beam is strongly coherent since up to the 10th order of diffraction from this grating is visible. The LAED patterns from crazes were scanned two-dimensionally by a computer-driven Joyce–Loebl microdensitometer using a 125 μm × 125 μm aperture. In this paper the x-direction is perpendicular to the craze fibrils (parallel to the craze-bulk interface) and the y-direction is parallel to the craze fibrils (perpendicular to the craze-bulk interfaces). The intensity on the plate was summed along lines parallel to the craze fibrils (y-direction). Each line corresponds to a certain scattering vector s, along the x-direction, perpendicular to the craze fibrils, where $|s| = 2\theta/\lambda$ and where θ is the scattering angle and λ is electron wavelength. The intensity $i(s)$ obtained in this fashion corresponds to that obtained using slit collimation in SAXS where the slit length is parallel to the fibril axis. The average fibril spacing, D_0, was estimated from the maximum position of the diffraction curves using Bragg's law while the fibril diameter, D, was

obtained by the Porod analysis on the high s portion of the diffraction curve [19, 34, 35].

The craze TEM images were analysed by computing the Fourier transform of the one-dimensional optical density distribution of the TEM image plate along the x-axis (i.e. perpendicular to the craze fibrils). Traces of the optical density distribution along the craze length were obtained from the microdensitometer using the 125 μm × 125 μm aperture and read into a computer at a displacement interval set externally. The transform of the fibril structure image was then computed by a fast Fourier transform computer program to generate the spectrum in the spatial frequency domain parallel to x-axis. The spectrum of the fibril images should show a maximum along the frequency axis, if there is any correlation between the fibril spacing. Clearly in order to reveal the fibril structure on the plates the displacement intervals between the readings of the microdensitometer during the scans should be significantly smaller than the fibril dimensions on the micrographs. From the LAED results the average craze fibril spacings and fibril diameters are in the range of 27 and 10 nm, respectively [31], and thus a 1.25 nm interval perpendicular to the fibrils, which corresponds to a 25 μm interval on the image at a magnification (M_g) of 20 000, was used. Each scan was 60 mm in length and usually five such scans equally spaced to fill the craze width were transformed individually; their spectra were summed to yield the final spectrum. The midrib [3] along the craze centre, which is produced by fibril drawing under stress concentration just behind the craze tip, has a much lower fibril volume fraction and was always avoided so that the data taken are representative of the average craze microstructure. The final spectrum obtained this way should then correspond to the LAED from the craze.

The optical transforms of the craze fibril images were generated by using the TEM images plates as diffraction masks on a laser optical bench. The laser beam was scattered during passage through a selected area on the TEM negative and the diffraction pattern was recorded on Polaroid film. The random scattering from the selected-area aperture edge, which can overlap with the optical transform, was avoided by using an aperture of suitable size, usually about 3 cm diameter. Dust particles, too, cause random scattering of the laser light thus increasing the noise background levels and should be eliminated from the lenses and mask.

Monodisperse polystyrenes (PS) purchased from Pressure Chemical Company were used throughout the experiments. Crazes in the PS with molecular weights of 18×10^5 and 11×10^4 were investigated by LAED and the Fourier transform microdensitometry (FTMD) methods. To compare optical transforms with LAED, crazes in a blend of 18×10^5 PS diluted 50% by volume with 2×10^3 monodisperse PS were examined along with those in the undiluted 18×10^5 PS.

3. Experimental results

Provided that the background intensity in LAED is very small, it can be shown that the three independent techniques employed here are indeed equivalent. The optical density, OD, in a small region on the TEM negative is linearly proportional to the electron dose received by that region when that dose is low. This behaviour of the coating emulsion on the TEM negatives has been verified [36] and used extensively, for example, in the measurement of the fibril extension ratio of the thin film crazes [14–16]. Since LAED is essentially the Fourier transform of the electron intensity exiting the craze, the Fourier transform of the optical density, OD, distribution on the TEM negative containing the craze image should be equivalent to LAED. On the other hand, when the light beam of the intensity i_0 travels through a small region of low optical density, OD, on the TEM negative, the optical density, OD, on the negative can be related by definition to the transmitted optical beam intensity, i_t, by the following equation:

$$OD = -\log [1 - (i_0 - i_t)/i_0] \quad (1)$$

Because the optical density is low, the quantity $(i_0 - i_t)$ is small enough that i_t can be expressed as

$$i_t = -ODi_0 + i_0 \quad (2)$$

Since the optical transform of the craze image is the root mean square of the Fourier modulus of i_t, it should be identical to the root mean square of the Fourier transform of the optical density except only at the origin in the frequency domain. The parameters of the fibril structure obtained from LAED, and from optical transform, or FTMD of images, thereby should be comparable.

LAED patterns from the fresh crazes in monodisperse 18×10^5 molecular weight PS are shown in Fig. 1. The streaks in the x-direction represent the scattering from the main craze fibrils. The angular splaying of the fibril scattering streaks through an angle ϕ results from a distribution of the angles between the main fibrils and the y-axis (tensile axis). This angular spread probably arises from the existence of cross-tie fibrils which connect the main fibrils. Two diffuse satellites along the y-direction are visible in Fig. 1. These are believed to be due to the scattering from a quasi-regular arrangement of these cross-tie fibrils [31]. The refraction streaks from the craze-bulk boundaries [37] are absent from the pattern because these boundaries were excluded by placing the selected-area aperture entirely within the craze.

The fibril scattering in the LAED patterns may be quantitatively represented by the slit smeared intensity, i, against the diffraction vector, s, curve, an example of which is shown in Fig. 2. The maximum is due to interfibrillar interference [19]. The average fibril spacing, D_0, can be estimated from the location, s_{max} in the $i(s)$ curve by assuming that [19]

$$D_0 \approx s_{max}^{-1} \quad (3)$$

This D_0 is an overestimate of the true average fibril spacing due to the fact that the fibril scattering intensity is proportional to the fourth power of the fibril size so that the interference between larger fibrils (larger spacings) is overweighted in the $i(s)$ curve [19]. The

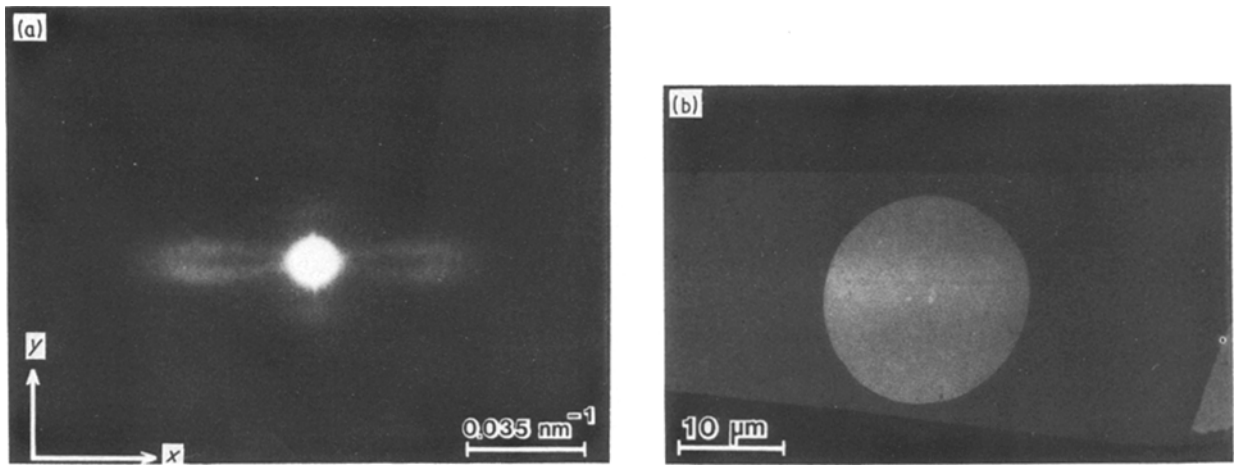

Figure 1 (a) Low-angle electron diffraction (LAED) pattern from a fresh, wide craze in monodisperse polystyrene ($M_w = 18 \times 10^5$). (b) TEM image showing the region selected for the LAED pattern in (a).

quantity s_{max}^{-1} is 28 nm for the crazes in 18×10^5 molecular weight PS.

The average fibril spacing, D_0, can be estimated in a different way which is believed to be more reliable. Since each fibril of diameter D can be regarded as being transformed plastically from a phantom fibril of diameter D_0, which must be also equal to the fibril spacing, D_0 can be calculated from the fibril diameter D and the fibril extension ratio, λ_{craze}, by making use of the fact that polymer volume is conserved during plastic drawing process [3], i.e.

$$(D_0/D) = (\lambda_{craze})^{1/2} \quad (4)$$

The fibril extension ratio, λ_{craze}, can be measured by optical microdensitometry of TEM image plates and is found to be a constant throughout the craze except in the midrib region. For PS air crazes, λ_{craze} was measured [32] to be approximately 4.0. The average fibril diameter, D, can be measured from the Porod constant, k_1, and Q, the small-angle scattering invariant, using [18]

$$D = \langle D^2 \rangle / \langle D \rangle = Q/[\pi^3(1 - v_f)k_1] \quad (5)$$

where v_f is the fibril volume fraction ($v_f = 1/\lambda_{craze}$). The Porod constant, k_1, was determined by extrapolating the value of is^3 in the Porod plot to $s = 0$ as shown in Fig. 3. The invariant Q can be calcuated using the equation

$$Q = 2\pi \int_0^\infty si(s)\,ds \quad (6)$$

For reliable results it is necessary to extend the integral to infinite s using the Porod constant, k_1, i.e.

$$Q = 2\pi \int_0^{s_p} i(s)\,s\,ds + 2\pi \int_{s_p}^\infty i(s)\,s\,ds \quad (7)$$

where s_p is a scattering vector in the regime where $i(s) = k_1/s^3$. Substituting the Porod value for $i(s)$ into the last integral results in

$$Q = 2\pi \int_0^{s_p} i(s)\,s\,ds + 2\pi k_1/s_p \quad (8)$$

The average craze fibril diameter, D, determined for crazes in 18×10^5 molecular weight PS is ~ 10 nm and the average fibril spacing from Equation 4 is thus approximately equal to 20 nm.

The Fourier transform microdensitometry (FTMD) method was calibrated and the computer program was tested by transforming the microdensitometer scan of a transparent ruler along its length. The Fourier spectrum of this "grating" correctly reflects the millimetre spacing of the ruler. TEM image negatives of a craze at two different magnifications, $\times 20\,000$ and $\times 50\,000$, were used for the initial FTMD trial analysis. For each plate, five parallel line scans uniformly spaced to cover the whole craze width were made on the craze image along the craze length, the x-axis. An example of such scans is shown in Fig. 4. The abscissa parameter, s_{image}, in the Fourier spectrum is defined as $2\pi/x$. The product of s_{image} with the image magnification, M_g, is equivalent to the scattering vector s in LAED.

The sum of the FTMD spectra from the five line scans is shown in Fig. 5 which demonstrates a strong maximum at $s_{image,max}$ corresponding to the periodicity of the optical density on the craze TEM images. Owing to the sizable noise associated with the main signal, the Fourier transformed data were smoothed by locally averaging data points (typically every ~ 25 points in a total of 1200 points). Fig. 6 shows the smoothed curves of the two magnifications, 20×10^3

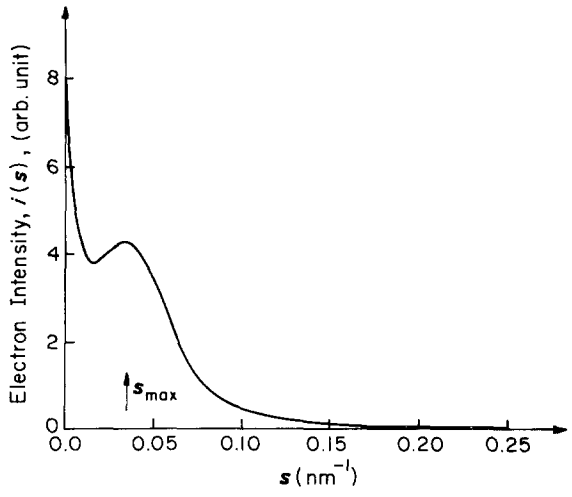

Figure 2 Slit smeared intensity curve of the LAED pattern in Fig. 1. The slit length is perpendicular to the horizontal streak.

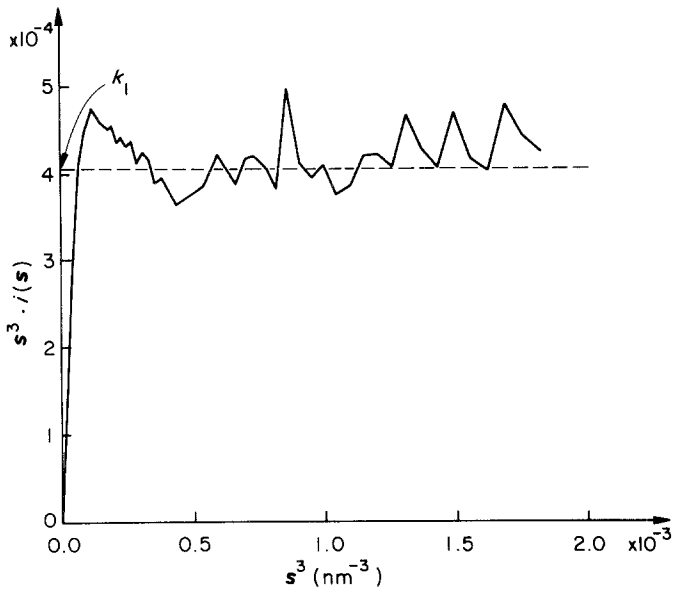

Figure 3 Porod plot of the slit smeared intensity in Fig. 2.

and 50 × 10^3. Although a smearing of approximately 1.5 nm should be introduced by this smoothing procedure, the fibril spacings measured from the two magnifications are in good agreement. The "diffracted intensity" obtained this way corresponds to a scanning point aperture across the LAED pattern, rather than the slit aperture used previously. For well-oriented fibrils the change in shape of the $i(s)$ curve should be minimal, however. This view is supported by the fact that the average fibril spacing, D_0, calculated from the value $s_{image,max}$ and M_g using Equation 3 is about 26 to 27 nm, only slightly smaller than that, 28 nm, determined by LAED.

Since the FTMD method relies on the quantitative information in the image rather than diffracted intensities, the defocus condition under which these images are taken inevitably influences the final spectra. In fact, because the Fresnel fringes at the edge of the fibril images disappear at true focus, these fibril images are not well defined under this condition and the FTMD spectrum of the in-focus craze fibrils becomes unresolved. The average fibril spacing from the maximum in the FTMD spectrum is plotted against underfocus in Fig. 7. The slight underfocus that is commonly used to enhance the visual quality of the images is necessary to produce a FTMD spectrum. Beyond that value $s_{image,max}$ is constant with defocus. The large noise in the FTMD spectrum means that the Porod analysis used to analyse the LAED patterns cannot be used here with certainty.

Unlike the FTMD analysis of the TEM images, which requires tedious computation, optical transform analysis of these images can provide the two-dimension Fourier transform rapidly. The effective camera constant of the optical transform was determined using the TEM images of a carbon waffle grating as calibration masks. The optical transform of the grating image is very similar to the LAED pattern from the same grating. Because we have the flexibility in choosing the magnification of the craze TEM plates, we can either increase the image magnification to reveal quantitative information from the fine structure in very small areas or lower the magnification to observe the diffraction patterns from a global region, provided that the contrast of the image permits. This flexibility is limited in some cases, however, by the appearance of some concentric dark rings which are superimposed on the diffracted intensity from the

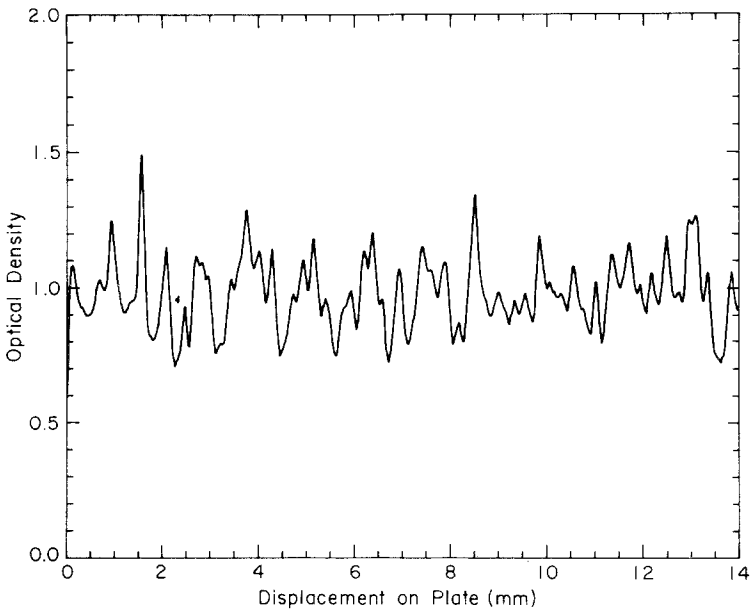

Figure 4 One-dimensional optical density distribution along the craze length in a TEM image plate (× 50 000) obtained from a microdensitometer scan.

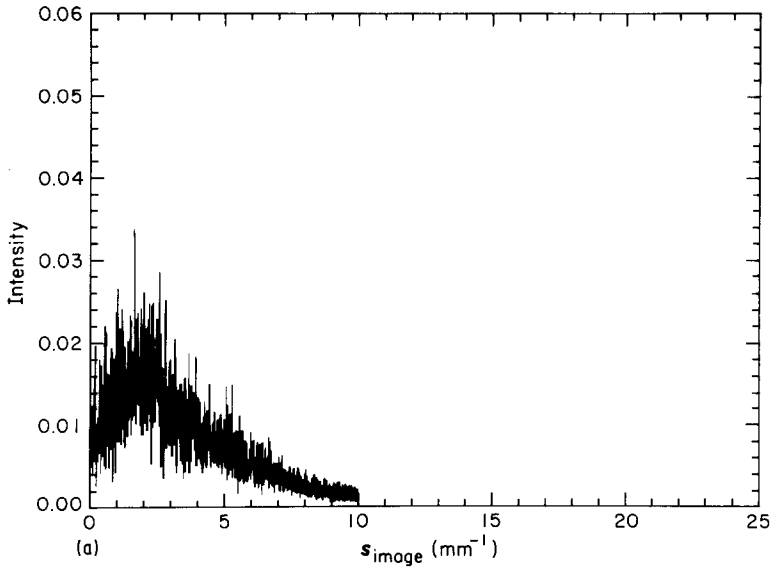

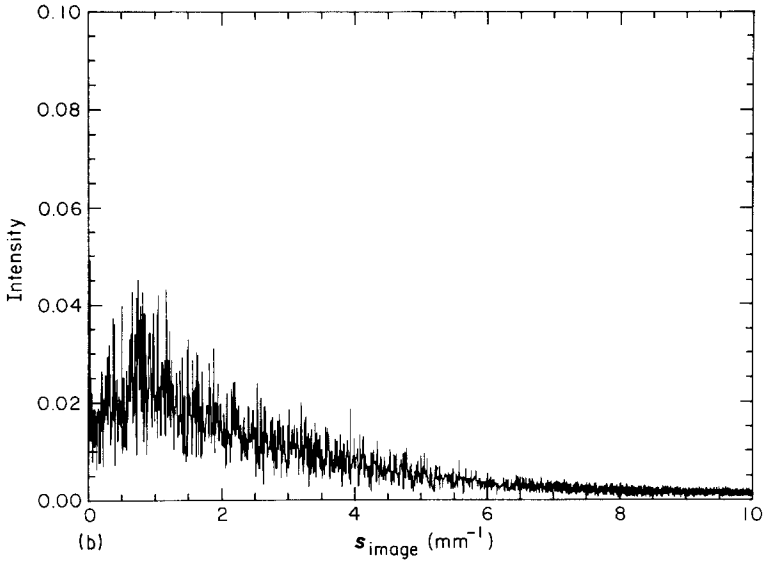

Figure 5 The sum of five FTMD spectra taken at various positions along the width of a craze for plates of magnification (a) $\times 20\,000$, (b) $\times 50\,000$. Intensity is in abitrary units.

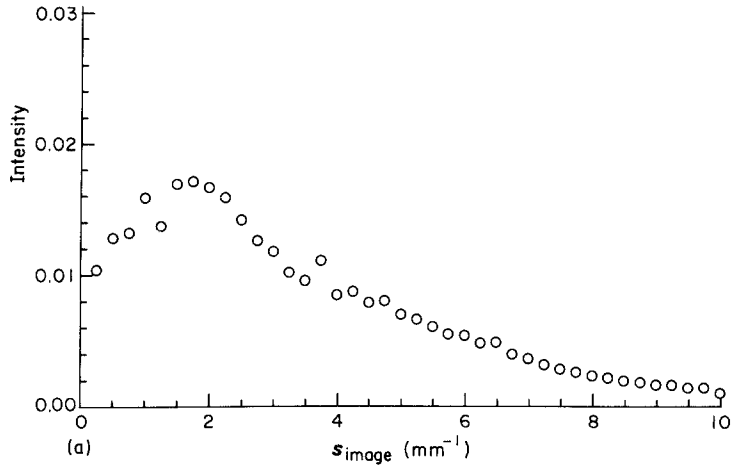

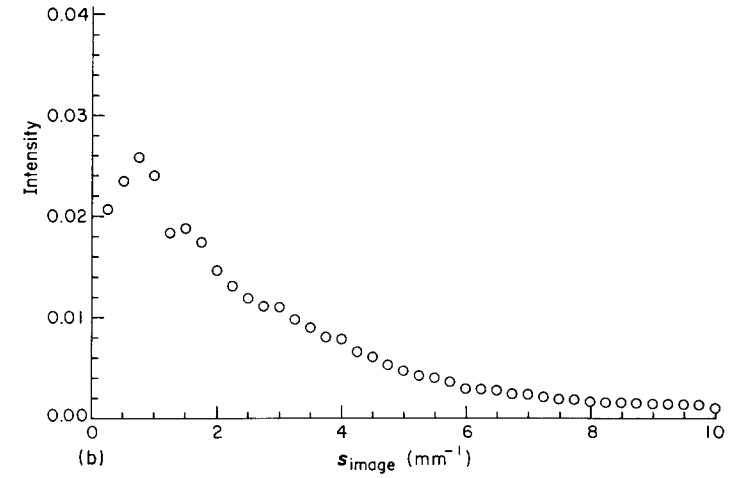

Figure 6 Smoothed FTMD spectra, by local averaging, of Fig. 5. (a) $\times 20\,000$, (b) $\times 50\,000$.

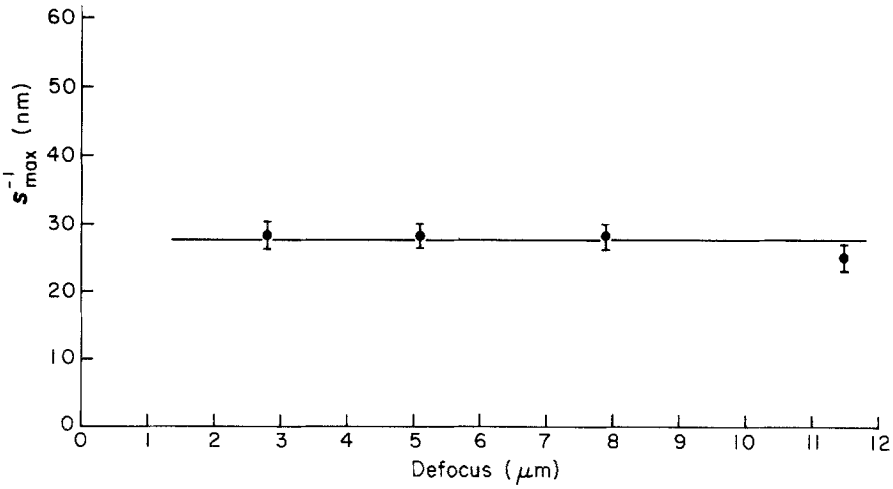

Figure 7 The average fibril spacing $D_0 = (s_{image,max})^{-1}$ from FTMD spectra taken from TEM plates recorded at various values of defocus.

craze fibrils. The rings, which disappear at zero defocus of the TEM, gradually shift in towards the origin as defocus increases. They are believed to be caused by the transfer function of objective lens of the transmission electron microscope, commonly called the "lens' transfer function". This defocus effect, which would not appear in LAED since the objective lens is essentially not energised, should be also present in the FTMD spectra. The large noise in these spectra, however, apparently prevents us from detecting it.

Fig. 8 shows a light scattering pattern from a TEM image of a craze in 18 × 10^5 PS at a magnification of × 5000. Although the outer part of the pattern is cut off by the first dark ring, we observe that it has the same features as of the LAED patterns from the same crazes (Fig. 2). While we could reduce the size of the optical tranforms to get rid of the defocus rings by increasing the image magnification, the selected-area aperture available is not large enough to include a relatively large area in the craze image on the higher M_g plates. To compare the optical transform patterns with the LAED patterns the area selected on the mask for light scattering should be large enough to cover the overall features of the craze fibril structure. An optical transform from the image at × 5000 can serve, however, for crazes which have larger fibril spacings.

From previous experiments [16] we know that when the short-chain oligomers are added to the high molecular weight PS, the crazes in the diluted entanglement network have a larger fibril spacing and the diffraction pattern shrinks. Fig. 9 shows the LAED patterns from a craze and the optical transform from the craze image in 18 × 10^5 PS diluted 50% with 2 × 10^3 PS. The LAED pattern and the optical diffraction pattern are very similar. The position of the maximum in the light scattering pattern can be measured directly from the film. When this is converted to a fibril spacing, the value of D_0 obtained is the same within experimental error as that measured by LAED. This equality holds for crazes in 18 × 10^5 PS (Fig. 8), as well as for those in the diluted 18 × 10^5 PS (Fig.9). The noise in the high s tail of the optical transform pattern prevents us from using the Porod analysis to obtain D.

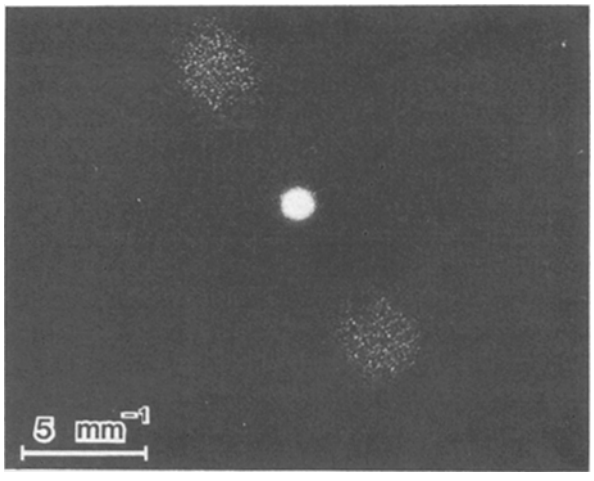

Figure 8 Optical transform of a TEM image of a fresh wide craze in monodisperse PS of 18 × 10^5 molecular weight.

The microstructure of crazes in 11 × 10^4 molecular weight PS was explored by LAED and FTMD image analysis. As illustrated by the LAED pattern shown in Fig. 10, the crazes in low molecular weight PS have fibrils with a narrower distribution of angles with respect to the tensile axis than do those in the high molecular weight PS (Fig. 1). The position of the maximum in $i(s)$, s_{max}, is closer to the transmitted beam than the s_{max} in the $i(s)$ from the crazes in high molecular weight PS (Fig. 10). There are also no diffuse satellites in the y-direction. These observations point to a lower density of tie fibrils in the crazes in 11 × 10^4 PS than in the crazes in 18 × 10^5 PS (Fig. 11). From Fig. 10b the value of s^{-1}_{max} for 11 × 10^4 PS is approximately 41 nm. If we compute a more accurate value of D_0 from Equation 4 with the fibril extension ratio λ_{craze} unchanged at a value of 4, the average fibril spacing, D_0, is found to be 25 nm for 11 × 10^4 PS compared to 20 nm for the 18 × 10^5 PS. The average fibril diameter, D, by Porod analysis is determined to be approximately 12 nm for the crazes in 11 × 10^4 PS, compared to 10 nm for the crazes in 18 × 10^5 PS. The fibril dimensions seem to be slightly larger in the low molecular weight PS.

However, the increase in the fibril diameter and spacing of the lower molecular weight PS may be due to fibril coalescence reported previously [31]. Crazes in 18 × 10^5 PS show D_0 and D values that increase with ageing. Although the 11 × 10^4 PS film squares examined were freshly prepared and cut from the copper grid, they were strained at a very low strain rate, 5 × 10^{-7} sec^{-1}, in order to achieve wide enough

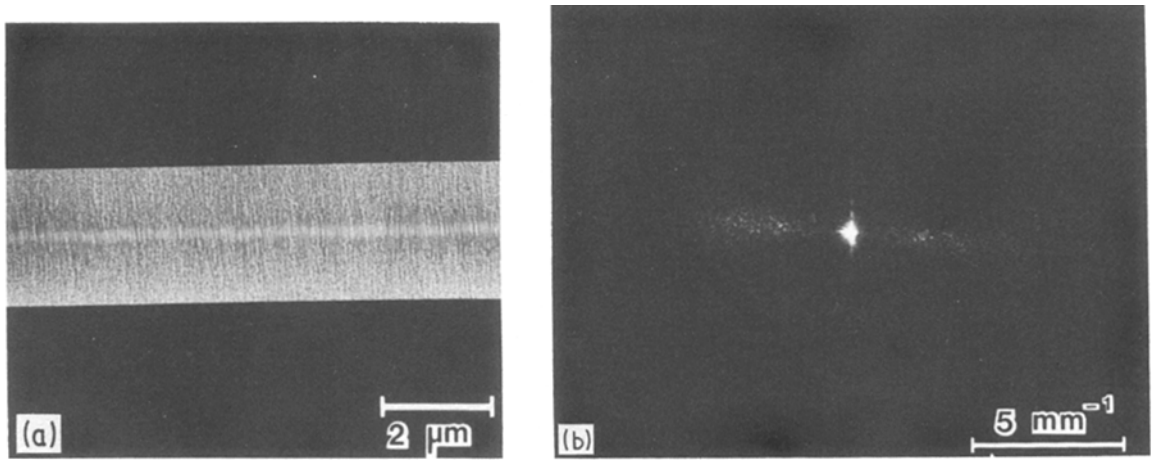

Figure 9 (a) TEM image of a craze in a blend of 50% 18 × 10^5 PS and 50% 2 × 10^3 PS; (b) optical transform of the image in (a); (c) LAED pattern of the same craze.

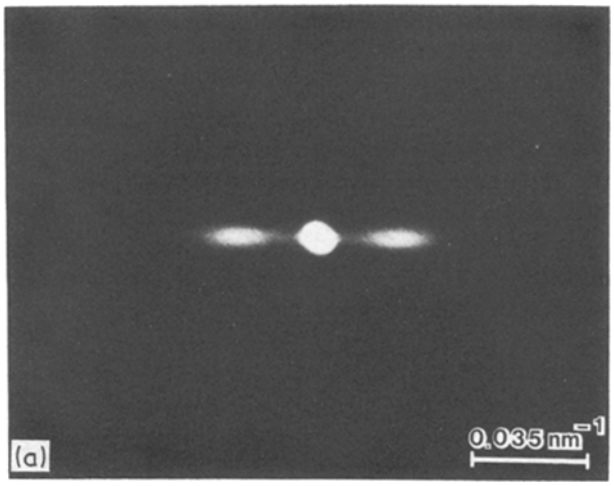

crazes to accept the whole selected-area aperture. Fibrils may have undergone progressive coalescence even during straining due to the shorter relaxation time of the shorter chains. Fibril dimensions are larger closer to the midrib where the fibril coalescence is most likely to take place. From Fig. 12, which shows s_{max}^{-1} obtained by FTMD at different y values along the craze width, we can observe that the fibril spacing increases towards the craze centre (midrib). The average fibril spacing varies from approximately 29 nm near the interface to about 50 nm near the centre, while the sum of the five scans gives an average fibril spacing of 34 nm for the whole craze.

4. Discussion

By comparing the craze low-angle electron diffraction (LAED) patterns with the Fourier transforms of images of the same craze it is clear that the information contained in the LAED pattern is not greatly distorted by the inelastic scattering background. The agreement between the three methods indicates that they are all

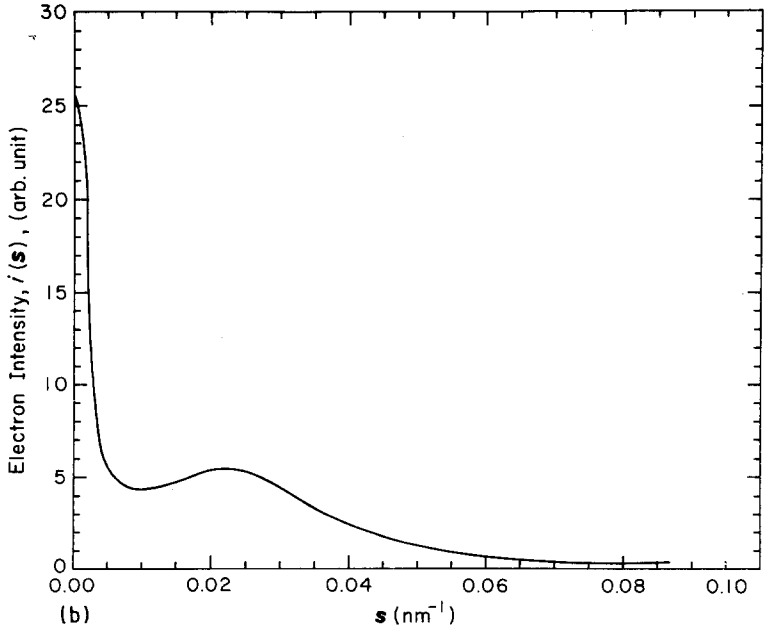

Figure 10 (a) LAED pattern of a fresh wide craze in monodisperse PS of 11 × 10^4 molecular weight. (b) The slit smeared intensity of the LAED pattern in (a).

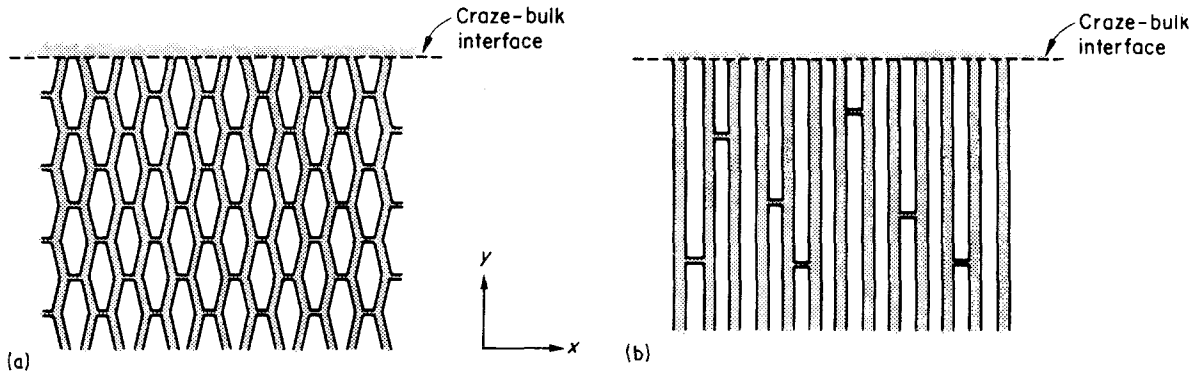

Figure 11 Schematic drawing of craze fibril structure of: (a) 18 × 10^5 PS, (b) 11 × 10^4 PS.

useful for craze microstructure characterization. Because of the many advantages stated in the previous paragraphs, LAED is a powerful and very attractive technique. However, we should point out that the results presented here do not lead to the conclusion that no inelastic component exists, only that it is apparently coherent enough over the crucial s range to give useful structural information through interference. Through the Porod analysis we found that there exists a uniform electron scattering background which was taken as the intensity far from the beam stop [31]. This uniform background is quite small compared to the main diffraction signals. There is also a possibility of an angle-dependent background component very close to the main beam. The existence of such a component would not change greatly the D values and would affect D_0 hardly at all.

The FTMD and optical transform analyses of electron images provide useful alternatives to LAED for craze structure determination in thin films and can function as an independent check on the results of LAED. The FTMD technique can be used to analyse the structure quantitatively without restrictions on the effective "camera length" or the "selected-area aperture size" as long as the resolution of the TEM permits the images to be obtained. This capability of FTMD makes it valuable when used along with LAED. It can also be expanded to have the power of handling the two-dimensional transforms, an extension which was not pursued here. But even with only the ability to determine one-dimensional transforms, the FTMD method is useful to probe the fine structure at various positions along the craze width, as illustrated above. However, the noise in the FTMD spectrum causes problems in performing analyses, such as the Porod analysis, where the signal of interest is small. On the other hand, although the optical transform analysis of image plates has equally serious noise problems, it also shares some of the advantages of the FTMD method. It can help one investigate the craze structure over a wide range of scales by yielding the two-dimensional diffraction patterns quickly and inexpensively. It is an ideal tool for a quick qualitative examination of the crazes of interest.

5. Conclusions

1. Low-angle electron diffraction is a useful and reliable method for exploring the craze fibril structure in thin films. The inelastic scattering background is shown to be very small compared to the main diffraction signal from crazes.

2. The craze TEM images can be directly examined by the methods of Fourier transform microdensitometry or optical transforms to yield equivalent quantitative information about the craze fibril structure.

3. The low molecular weight (11 × 10^4) crazes examined here have slightly larger average fibril diameters and fibril spacings compared to those of the high molecular weight PS. The difference is most likely due to more rapid fibril coalescence in the lower molecular weight crazes. Fewer cross-tie fibrils are formed during craze widening in the low molecular weight PS than during craze widening in the high molecular weight PS, giving rise to more nearly perfect fibril orientation in the former case.

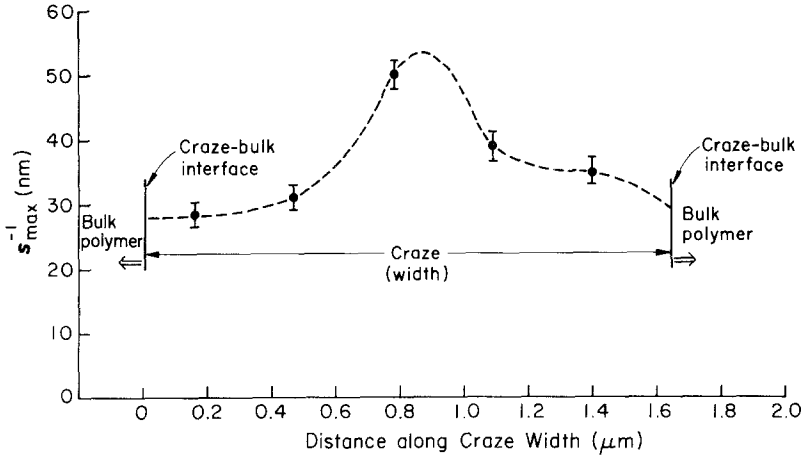

Figure 12 Average fibril spacings (s_{max}^{-1}) in 11 × 10^4 PS at various positions along the width of a wide craze from its FTMD spectra.

Acknowledgements

We gladly acknowledge the financial support of the Army Research Office-Durham and the use of the facilities of the Cornell Materials Science Center which is funded by NSF-DMR-MRL Program. We thank Professor C. B. Carter for allowing us to use his laser optical bench and B. de Cooman for helpful discussion on the optical method of analysing TEM images.

References

1. R. P. KAMBOUR, *J. Polym. Sci. Macromol. Rev.* **7** (1973) 1.
2. S. RABINOWITZ and P. BEARDMORE, *CRC Rev. Macromol. Sci.* **1** (1972) 1.
3. E. J. KRAMER, *Adv. Polym. Sci.* **52/53** (1983) 1.
4. A. N. GENT, "The Mechanics of Fracture", Applied Mechanics Division, Vol. 19, edited by F. Erdogon (American Society of Mechanical Engineers, New York, 1976) p. 55.
5. E. J. KRAMER, *Polym. Eng. Sci.* **24** (1984) 761.
6. A. C.-M. YANG and E. J. KRAMER, *Bull. Amer. Phys. Soc.* **29** (1984) 531.
7. A. N. GENT and A. G. THOMAS, *J. Polym. Sci. A2* **10** (1972) 571.
8. S. WELLINGHOFF and E. BAER, *J. Macromol. Sci. Phys.* **B11** (1975) 367.
9. T. E. BRADY and G. S. Y. YEH, *J. Mater. Sci.* **8** (1973) 1083.
10. G. L. PITMAN and I. M. WARD, *Polym.* **20** (1979) 895.
11. R. P. KUSY and D. T. TURNER, *ibid.* **18** (1977) 391.
12. P. PRENTICE, *ibid.* **24** (1983) 344.
13. H. W. McCORMICK, F. M. BROWER and L. KIN, *J. Polym. Sci.* **39** (1959) 87.
14. A. M. DONALD and E. J. KRAMER, *J. Polym. Sci. Polym. Phys.* **20** (1982) 899.
15. *Idem, Polymer* **23** (1982) 461.
16. A. C.-M. YANG, E. J. KRAMER, C. C. KUO and S. L. PHOENIX, *Macromol.*, in press.
17. A. M. DONALD, T. CHAN and E. J. KRAMER, *J. Mater. Sci.* **16** (1981) 669.
18. E. PAREDES and E. W. FISCHER, *Macromol. Chem.* **180** (1979) 2707.
19. H. R. BROWN and E. J. KRAMER, *J. Macromol. Sci. Phys.* **B19** (1981) 487.
20. H. R. BROWN, *J. Polym. Sci. Polym. Phys.* **21** (1983) 483.
21. H. MAHL and W. WEITSCH, *Naturwiss.* **46** (1959) 487.
22. *Idem, Z. Naturforsch.* **15a** (1960) 1051.
23. *Idem, Optik* **17** (1960) 487.
24. R. P. FERRIER, in "Advances in Optical and Electron Microscopy", Vol. 3, edited by E. Baser and V. E. Cosslett (Academic, London, 1969) p. 155.
25. W. T. SCOTT, *Rev. Mod. Phys.* **35** (1963) 231.
26. J. SMART and R. E. BURGE, *Nature, Lond.* **205** (1965) 1297.
27. J. M. COWLEY, "Diffraction Physics" (North-Holland, Amsterdam, 1975).
28. F. LENZ, *Z. Naturforsch.* **9a** (1954) 185.
29. M. T. TOMPSETT, M. B. HERTAGE and C. W. B. GRIGSON, *Nature, Lond.* **215** (1967) 29.
30. G. H. CURTIS and R. P. FERRIER, *Proc. Electron Microsc. Soc. Amer.* **27** (1969) 154.
31. A. C.-M. YANG and E. J. KRAMER, *J. Polym. Sci. Polym. Phys.* **23** (1985) 1353.
32. B. D. LAUTERWASSER and E. J. KRAMER, *Phil. Mag.* **A39** (1979) 469.
33. A. M. DONALD and E. J. KRAMER, *J. Mater. Sci.* **16** (1981) 2967.
34. G. POROD, *Kolloid Z.* **124** (1951) 83.
35. *Idem, ibid.* **125** (1952) 109.
36. B. D. LAUTERWASSER, PhD thesis, Cornell University (1979).
37. H. R. BROWN, *Ultramicroscopy* **7** (1982) 263.

Received 5 November
and accepted 20 December 1985